PHYSICAL RETRIEVAL OF PRECIPITATION WATER CONTENTS FROM SPECIAL SENSOR MICROWAVE/IMAGER (SSM/I) DATA-PART II: RETRIEVAL METHOD AND APPLICATIONS (report version)

by

William S. Olson

Cooperative Institute for Meteorological Satellite Studies

1225 West Dayton Street

University of Wisconsin

Madison, Wisconsin 53706

To be modified and submitted to *J. Appl. Meteor.*

PHYSICAL RETRIEVAL OF PRECIPITATION WATER CONTENTS FROM SPECIAL SENSOR MICROWAVE/IMAGER (SSM/I) DATA- PART II: RETRIEVAL METHOD AND APPLICATIONS (report version)

by

William S. Olson

1. INTRODUCTION

The retrieval of precipitation distributions by passive microwave techniques has been an area of study in satellite remote sensing for well over a decade. The recent initiative to estimate both the horizontal and vertical distributions of precipitating liquid water in the tropics, i.e. the Tropical Rainfall Measuring Mission or TRMM, has further stimulated interest in this area; see Simpson, et al. (1988). The proposed TRMM satellite will carry a suite of sensors including passive and active microwave instruments, as well as visible and infrared radiometers. In addition to TRMM, a combination of microwave and visible/IR sensors has also been proposed for the Earth Observing System (EOS) platforms for the purpose of retrieving rainfall rates and other geophysical parameters; ref. Schoeberl, et al. (1992). Methods for determining precipitation distributions based upon data from several instruments having different spectral and resolution characteristics will therefore be required.

Currently multispectral microwave observations from the Special Sensor Microwave/Imager (SSM/I), borne by the DMSP-F8, F10, and F11, have provided researchers with the means for retrieving rainfall rates; see Hollinger (1991), Kummerow, et al. (1989), Petty and Katsaros (1990), Xiang, et al. (1992). The SSM/I is a multichannel, dual-polarization, passive microwave radiometer with channels at 19.35, 22.235, 37, and 85.5 GHz. The diffraction limitation of the SSM/I antenna causes the spatial resolution of measurements to increase with frequency, such that the minimum footprint dimension decreases from 43 km at 19.35 GHz to 13 km at 85.5 GHz. The DMSP-F8, F10, and F11 also carry the Special Sensor Microwave/Temperature (SSM/T) sounder with channels at 50.5, 53.2, 54.35, 54.9, 58.4, 58.825, and 59.4 GHz, and a

footprint dimension of approximately 180 km at nadir view. In addition the DMSP F11 carries the Special Sensor Microwave/Temperature -2 (SSM/T-2) sounder, with channels at 91.665, 150, and 183.3 ± 1, ± 3, ± 7 GHz, and a minimum footprint dimension of 48 km at nadir view. The SSM/T and SSM/T-2 can provide temperature and humidity information not available from the SSM/I alone.

In the present study, a physical retrieval method for estimating precipitating water distributions and other geophysical parameters based upon measurements from the DMSP-F8 SSM/I is developed. Three unique features of the retrieval method are (1) sensor antenna functions are explicitly included to accommodate varying channel resolution, (2) precipitation-brightness temperature relationships are quantified using the cloud ensemble/radiative parameterization described in Part I, and (3) spatial constraints are imposed for certain background parameters, such as humidity, which vary more slowly in the horizontal than the cloud and precipitation water contents. The general framework of the method will facilitate the incorporation of measurements from the SSM/T, SSM/T-2 and geostationary infrared measurements, as well as information from conventional sources (e.g. radiosondes) or numerical forecast model fields.

2. METHOD

The basis of the retrieval method is the minimum variance solution as described in Lorenc (1986). An error functional which expresses the deviation of the observed satellite antenna temperatures from model-derived values, plus an additional constraint which represents the deviation of retrieved geophysical parameters from *a priori* estimates, is derived.

$$E = (\mathbf{TA}_{obs} - \mathbf{TA(P)}_{mod})^T \Sigma^{-1} (\mathbf{TA}_{obs} - \mathbf{TA(P)}_{mod}) + (\mathbf{P} - \mathbf{P}_{apriori})^T \Delta^{-1} (\mathbf{P} - \mathbf{P}_{apriori}) \quad (1)$$

Here, $\mathbf{TA}_{obs}$ is a vector of antenna temperature measurements, $\mathbf{TA(P)}_{mod}$ are antenna temperature estimates based on the sensor response model (see Part I of this series), **P** is a vector of geophysical parameters to be retrieved, and $\mathbf{P}_{apriori}$ are estimates of the parameters based upon *a priori* knowledge. Σ and Δ are covariance matrices representing observational plus model errors (Σ), and errors in the *a priori* estimates (Δ). In the present study all off-diagonal elements of these matrices are neglected.

The retrieval of precipitating liquid water contents and other geophysical parameters is accomplished by iteratively perturbing the geophysical parameters until the error functional Eq. (2) is minimized. Unlike Lorenc (1986), the error functional is minimized using the memoryless, quasi-Newton method described by Shanno (1978). The quasi-Newton approach is computationally efficient when the retrieval problem requires the simultaneous optimization of a large number of unknown geophysical parameters. In this situation, matrix inversion methods are impractical.

3. APPLICATION OF THE RETRIEVAL METHOD TO SSM/I DATA

3.1 Retrieval Parameters and Constraints

In Part I of this series, a sensor response model was developed for SSM/I to relate measured microwave antenna temperatures to variations in geophysical parameters in the earth/atmosphere system. The sensor response model is designated $\mathbf{TA(P)}_{mod}$ in Eq. (1). The explicit dependence of antenna temperature on slant path-integrated liquid and ice-phase precipitation, fractional coverage of liquid and ice precipitation within a 25 km x 25 km grid box, atmospheric temperature and water vapor, and surface temperature and emissivity were discussed in Part I. Although each of these geophysical parameters can have a significant effect on SSM/I antenna temperatures, only a limited number of unknown parameters can be allowed in the minimization of the error functional Eq. (1). Otherwise, ambiguous solutions can result.

Of primary interest are the distributions of precipitating liquid and ice over the swath grid, and therefore the slant path-integrated preciptitating liquid and ice, and the associated grid-box fractions are allowed to vary in the retrievals. Although variations in surface skin temperature and emissivity can affect microwave surface emission, climatological variations of surface skin temperature are relatively small. Surface skin temperature over the ocean varies by less than ± 5 K in the tropics, up to about ± 10 K at midlatitudes (Pickard and Emery, 1982). Any error in the retrieved value of skin temperature can easily be compensated by a change in the surface emissivity to produce nearly the same surface emission. Therefore, in this study the value of surface skin temperature is prescribed at a climatological value representative of the tropics (300.15 K). A somewhat better estimate could be obtained from infrared retrieval composites, but a climatological value is found to be sufficiently accurate for the purpose of demonstrating the retrieval method. Surface emissivities are parameterized according to the model of Grody (1988). The emissivity in each polarization has a frequency dependence given by

$$e = a + b \cdot \ln(\nu) \tag{2}$$

where ν is the channel frequencey and a and b are free parameters. Separate emissivity parameters describing the emissivities of land and ocean surfaces are allowed to vary in the retrieval, but it is assumed that these parameters are the same for every grid box of the swath grid. To account for the mixture of emissivities in grid boxes which contain both land and water surfaces, an additional land fraction parameter, f_{land}, is also allowed to vary in the retrieval. The effective emissivity is given by

$$e_{effective} = f_{land} \cdot e_{land} + (1 - f_{land}) \cdot e_{ocean} \tag{3}$$

In the retrieval method, profiles of atmospheric temperature and water vapor mixing ratio are represented by a mean profile and a set of profile eigenfunctions. The mean profiles and eigenfunctions are derived from a global radisonde data base of 1200 profiles developed by Smith, et al. (1974).

A link between the atmospheric profiles and cloud ensemble/radiative parameterization is established as follows. A profile of temperature and humidity (water vapor mixing ratio) is selected to serve as the environment for the cloud model simulations and ensemble generation described in Part I. The relationship between the generated ensembles and the computed upwelling microwave brightness temperatures is parameterized, and a set of fitting constants is calculated for that particular environment (see also Part I). Additional profiles of atmospheric temperature and humidity can be selected to generate cloud ensemble/radiative parameterizations appropriate for other climatologies.

In the retrieval, an initial guess profile is compared to all of the profiles utilized to generate cloud ensemble/radiative parameterizations. The parameterization associated with the profile which best matches the initial guess profile (in the mean-square sense) is selected for the retrieval of precipitation amounts in a given grid box. The guess profiles are allowed to deviate from the parameterization profiles by allowing the weighting of the first eigenfunctions of temperature and mixing ratio (in an eigenfunction decomposition of the guess profiles) to vary in the retrieval.

In the present study, the GATE Day 261 profile (ref. Ferrier and Houze, 1989) is selected to yield a cloud ensemble/radiative parameterization representative of tropical conditions. This single profile is selected for the demonstration of the precipitation retrieval method, since the applications herein include SSM/I observations of a tropical squall line and a developing tropical storm. However, cloud ensemble/radiative parameterizations corresponding to other temperature and humidity environments could be added to represent midlatitude conditions or other climatologies.

Physical retrieval tests in which the temperature and mixing ratio eigenfunction weights were allowed to vary in each grid box resulted in a lack of constraint on solutions and ambiguous retrievals. Ambiguous solutions were due to the fact that temperature variations and mixing ratio variations over land produce only a very small signal in upwelling microwave brightness temperatures at the SSM/I frequencies, and these signals are generally indistinguishable from variations in background emissivity or precipitation amount.

The ambiguities are removed by prescibing the first eigenfunction weight of temperature over the entire swath grid, and allowing the first eigenfunction weight of water vapor mixing ratio to vary only over oceanic regions. Over land, the first eigenfunction weight of mixing ratio is again prescribed.

Regarding the retrieval of precipitation parameters, preliminary testing also revealed an ambiguity between slant path-integrated precipitating ice and the fraction of precipitating ice within each grid box. The ambiguity in these retrieved quantities is removed by setting the fraction of precipitating ice equal to the fraction of precipitating liquid. This constraint is likely to introduce some error into retrieved precipitation amounts, since precipitating ice, which is associated with stronger convective updrafts and organized mesoscale motions (see Part I), generally has an areal extent which is different from the areal extent of precipitating liquid. The ice content/fraction ambiguity might be removed with the addition of higher-frequency ice sensitive channels on future microwave sensors.

A summary of parameters **P** in the SSM/I physical retrieval and the associated constraints on the parameters is summarized in Table 1.

In the initial demonstration of the retrieval method which is documented here, only the cloud ensemble/radiative parameterization based upon the GATE Day 261 profile is considered. This parameterization is appropriate since only retrievals of precipitation in the tropics are considered here. Precipitation retrieval applications in other climatic

environments, and the selection of alternative cloud ensemble/radiative parameterizations appropriate to those environments, will be the subject of a future study.

Estimates of observational and cloud ensemble/radiative parameterization errors are specified in the diagonal elements of Σ of Eq. (1). The observational error standard deviations of each SSM/I measurement are taken to be 3 K as suggested by Hollinger, et al. (1991) for absolute calibration errors. Parameterization error standard deviations are assumed to be 6 K in the 85.5 GHz channels and 3.6 K in the remaining channels. These figures reflect the greater residual errors in the 85.5 GHz parameterization fits to the cloud ensemble/radiative calculations of brightness temperatures (see Part I). An additional weighting factor of 0.25 is applied to the 85.5 GHz terms in Eq. (1) to compensate for the SSM/I 85.5 GHz sampling, which is four times as great as the sampling in the other channels.

The minimization of E in Eq. (1) requires the evaluation of finite difference derivatives of brightness temperatures with respect to the parameters **P**. Efficient convergence to a minimum requires that these derivatives be scaled to compensate for variations in sensitivity of brightness temperature to a particular parameter. Appropriate scaling factors for each parameter are selected based upon extensive retrieval tests.

3.2 Darwin Case Study

The physical retrieval method, Eq. (1), is applied to SSM/I observations of a tropical squall line at 0906 UTC on February 9, 1988 in the vicinity of Darwin, Australia. SSM/I observation of the squall line at 37 GHz and 85.5 GHz in the horizontal polarization are shown in Figs. 1a and 1b, respectively. In the panels of the figure, the northern coast of Australia and the outlines of Bathurst and Melville Islands are indicated by white lines, and the grayscale of brightness temperature values in K is displayed at the bottom. Each panel has dimensions of approximately 240 km x 240 km. The convective leading edge of the squall line parallels the coast of Australia, and is indictated by a line of relatively low brightness temperatures in the 85.5 GHz channel. These depressed brightness

temperatures are induced by the scattering of microwave radiances by precipitation-sized ice particles which are held aloft by relatively strong updrafts within the convective zone. A sequence of radar imagery from the Darwin/TOGA radar bracketing the SSM/I overpass time indicates a general southeast to northwest motion of the squall line (Steiner, 1992). A broad, trailing stratiform precipitation region to the south and east of the convective leading edge is seen as a relatively uniform depression in the 37 and 85.5 GHz brightness temperatures extending beyond the lower edge of each panel. The brightness temperatures in the trailing stratiform region tend to be higher than in the convective zone, which suggests that the concentrations of scattering ice particles are not as high in the stratiform zone. Regions of smaller-scale convective precipitation are seen as scattering depressions in the 85.5 GHz imagery to the northwest of the squall line, between Bathurst and Melville Islands, and also to the west of the convective line.

The SSM/I retrieval method is applied to a 64 x 64 section of the swath grid centered on the Darwin/TOGA radar site, located at the center of the panels in Fig. 1. All seven of the SSM/I channels are included in the retrieval. After 21 iterations of the quasi-Newton procedure the error functional E in Eq. (1) is effectively minimized without any additional constraints (second term equal to zero) to produce the retrievals of average slant path-integrated precipitating liquid and precipitating ice depicted in Figs. 2a and 2b, respectively. The image intensity in these panels is proportional to the equivalent column-integrated liquid water or ice from the retrieval. A grayscale relating depth-integrated water in kg/m^2 to image intensity is shown at the bottom of each panel.

From Fig. 2, it may be noted that the highest concentrations of integrated liquid precipitation occur along the convective leading edge of the squall line, with lower values spread almost uniformly over the trailing stratiform region. Peak values are close to 4 kg/m^2 in the convective leading edge, with typical values between 1 and 2 kg/m^2 in the trailing stratiform region. Regions of liquid precipitation associated with the convective zones west and northwest of Darwin are also seen in the retrieval. Retrievals of the

column-integrated precipitating ice in Fig. 2b exhibit relatively high values in both the convective leading edge and stratiform zones, on the order of 1 to 1.5 kg/m^2. The retrievals in the convective and stratiform zones have roughly the same magnitude, in contrast to the retrievals of liquid precipitation, which exhibit greater values along the convective leading edge. Also, the maximum ice amounts in the stratiform zone tend to be concentrated to the southeast of Darwin. Precipitating ice amounts are significantly less in the convective regions northwest and west of Darwin, with maximum values of about 0.8 kg/m^2.

A nearly concident radar volume scan from the 5-cm Darwin/TOGA radar starting at 0850 UTC on February 9, 1988 is processed to obtain comparative estimates of integrated liquid and ice precipitation amounts. The radar reflectivities from the volume scan are first interpolated to a cartesian grid with overall dimensions 240 km x 240 km x 18 km. The grid spacings are 2 km in the horizontal and 1.5 km in the vertical. The radar data in elevation/azimuth/range format are interpolated to grid locations using the method of Mohr and Vaughan (1979).

Within the convective leading edge of the squall line, the fractions of liquid and ice precipitation associated with a given radar reflectivity are estimated using the temperature-dependent partitioning scheme of Moss and Johnson (1992). Within the trailing stratiform region, it is assumed that the radar reflectivity is due entirely to ice-phase hydrometeors above the freezing level, and below the 6 C level the radar reflectivity is due entirely to liquid hydrometeors. A linear transition from ice to liquid between 0 C and 6 C is assumed. This stratiform precipitation partitioning scheme is based upon model simulations of anvil clouds using a one-dimensional version of the Ridout (1991, 1993) model. The vertical profile of environmental temperatures is obtained from the Darwin sounding at 2200 UTC on February 9, 1988.

Slant path-integrated liquid and ice-phase precipitation fields derived from the Darwin volume scan are shown in Figs. 3a and 3b, respectively. Fig. 3a may be compared to the

SSM/I retrieval of integrated liquid precipitation in Fig. 2a. Precipitation amounts in the convective leading edge and trailing stratiform regions of the tropical squall line have roughly the same magnitudes in both the SSM/I and radar estimates. A small positive bias in liquid precipitation estimates is evident in the SSM/I retrievals, however. Also, there appear to be spurious retrievals of light preciptation north of the squall line and along the lower edge of Melville Island. The high bias and spurious retrievals may be due, in part, to the lack of explicit nonprecipitating clouds in the cloud ensemble/radiative parameterization. The effect of nonprecipitating clouds is imbedded in the relationships between precipitation amount and upwelling brightness temperature, but the cloud liquid water content does not vary as an independent variable. A region containing significant nonprecipitating cloud can therefore be interpreted as a region of light precipitation in the retrieval. Spurious retrievals of liquid precipitation in coastal regions could also be due to slight errors in SSM/I data geolocation, coupled with the very low sensitivity of the SSM/I channels to variations in precipitating water in coastal regions. Although the SSM/I geolocation was checked and adjusted to match up with a coastline data base, any small error which would move the SSM/I data from land over ocean would require a large adjustment in the land fraction, f_{land}, to compensate. An increase in the amount of liquid precipitation in the retrieval solution could also provide this compensation. In addition, the derivative scaling for liquid precipitation in the vicinity of coastlines must be adjusted to compensate for the lack of sensitivity of upwelling brightness temperatures to variations in precipitating liquid amount. This is because the derivative goes through a change of sign and actually vanishes at a coastal boundary, and therefore derivative magnitudes are relatively small. The scaling of derivatives heightens the sensitivity of the parameterized brightness temperatures to changes in precipitating liquid, and leads to exaggeration of errors in the liquid precipitation retrievals arising from noise or improper geolocation.

The radar-derived slant path-integrated precipitating ice in Fig. 3b may be compared to the SSM/I retrieval in Fig. 2b. There is a fairly good correspondence between the radar and SSM/I retrieved fields, both in pattern and magnitude of precipitating ice. The figures suggest only a slight high bias of the SSM/I retrieved ice amounts over the radar estimates. Note that within about 20 km of the radar site there is a conical data-void region in the radar-derived field, due to the 25° limiting elevation angle of the radar (Keenan, et al., 1988).

3.3 Tropical Storm Emily - 1004 UTC Overpass

The physical retrieval method is applied to SSM/I observations of the incipient Tropical Storm Emily at 1004 UTC on September 21, 1987, as it was developing over the Windward Islands off the northeast coast of South America. The SSM/I 37 GHz and 85.5 GHz horizontal polarization images of Emily on this date are shown in Fig. 4a and 4b, respectively. The northern coast of South American and Caribbean Islands are indicated by white lines, and a brightness temperature grayscale is displayed at the bottom of each panel. The panel dimensions are approximately 1400 km x 1400 km. The most intense convective development in Emily is seen just north of the island of Trinidad and Tobago. This oblong convective zone spans about 250 km, with 37 GHz horizontal polarization antenna temperatures near 255 K, indicating strong absorption and emission from precipitating liquid. Embedded in the convective zone are smaller regions of microwave scattering at 85.5 GHz, especially to the north-northeast of Trinidad and Tobago. The more intense scattering regions are associated with precipitating ice held aloft by the stronger updrafts of the convective zone, and the 85.5 GHz horizontal polarization antenna temperatures reach a minimum of 150 K. To the north and northwest of the convective zone are semi-circular bands in the antenna temperature imagery arising from developing bands of precipitation. Most of these bands contain significant amounts of precipitating ice, identified by scattering depressions in the 85.5 GHz antenna temperatures.

The retrieval algorithm is applied to a 64 x 64 swath grid section centered on Emily. After 21 iterations the error functional in Eq. (1) is minimized to yield the retrievals of grid box average, slant-path integrated precipitating liquid and ice in Figs. 5a and 5b. It may be noted that the pattern of precipitating liquid in Fig. 5a closely follows the pattern of 37 GHz emission in Fig. 4a. Maximum values of integrated liquid occur in the convective core area of Emily, with magnitudes close to 2.6 kg/m^2, and lesser amounts, on the order of 1 kg/m^2, in developing rainbands. Retrievals of precipitating liquid along the coast of South America are spurious, for the most part, since coincident infrared imagery (not shown) at the time of the SSM/I overpass does not show significant cloud along the coast. The precipitation artifacts are likely due to a compensation in the retrieval for variations in land surface emissivity.

Integrated precipitating ice concentrations in the retrieval of Fig. 5b coincide with regions of strong scattering in the 85.5 GHz SSM/I imagery. Precipitating ice retrievals exhibit maximum values close to 3 kg/m^2 in the convective core region, with values up to 1 kg/m^2 in the outer bands. The overall extent and magnitude of the precipitating ice amounts are generally less than those of precipitating liquid in Emily at the overpass time.

3.4 Tropical Storm Emily- 2242 UTC overpass

The SSM/I retrieval procedure is repeated for a subsequent overpass of Emily at approximately 2242 UTC on September 21, 1987. SSM/I imagery from this overpass in the 37 GHz and 85.5 GHz horizontal polarization channels is shown in Figs. 6a and 6b, respectively. These may be compared to the imagery of Emily roughly 12 hours earlier, shown in Figs. 4a and 4b. It may be noted from the figures that the core region of Emily had moved about 400 km to the west-northwest of its original position in the Windward Islands. Also, the storm had taken on the classical structure of a hurricane, with spiral bands and an apparent eye which can be seen in the 85.5 GHz imagery. At the time of the second SSM/I overpass, Emily was still classified as a tropical storm, but was deepening

rapidly, and the storm attained hurricane status early the following day (ref. Case and Gerrish, 1988).

Retrievals of slant-path integrated precipitating liquid and ice from the second overpass of Emily are diplayed in Figs. 7a and 7b, respectively. A correspondence between precipitating liquid and 37 GHz emission patterns (Figs. 6a and 7a) is evident. Also there is a strong correlation between scattering depressions in brightness temperature and retrieved precipitating ice amounts (Figs. 6b and 7b), as it was noted in the 1004 UTC Emily retrievals. Maximum retrieved values of precipitating liquid and ice within Emily are on the order of 2 kg/m^2, although liquid precipitation amounts tend to be higher in general.

4. EXTENSION OF CURRENT WORK AND APPLICATIONS

Work will continue to further improve the representation of clouds and their environments in the sensor response model. Greater variability in the solution fields of emissivity, air temperature, and water vapor may also be allowed if additional sensor data and/or constraints are utilized in the retrieval. Future tests will include the lower-frequency SSM/I data as well as SSM/T, SSM/T-2, and geostationary infrared measurements. Retrievals will be validated using volume-scan radar measurements and conventional weather data.

The sequence of Emily retrievals is utilized in the latent heating analysis and numerical weather prediction model forecasts in Section 4 of this report. Rates of latent heating are inferred from the liquid and ice precipitation distributions and are assimilated into the forecast model fields using a new technique. This application is important because the development or "spin-up" of storms in numerical model forecasts is often retarded due to a lack of fine-scale initial data. The SSM/I-derived latent heating information can partially compensate for this lack of fine-scale data.

Latent heating information may help to improve short-term numerical weather prediction model forecasts of storms, but forecast model fields may also be used to help

improve retrievals through the constraint term in Eq. (1). The interplay between forecast models and retrievals is a subject of further study by the author.

Acknowledgments

The authors wish to thank Robert Aune, John Derber, Brad Ferrier, George Diak, Barry Hinton, James Hollinger, Christian Kummerow, Lynn McMurdie, Grant Petty, Gene Poe, Robert Rabin, James Ridout, David Short, Bill Smith, James Weinman, Mark Whipple and Harold Woolf for their help and inspiration during various phases of this study. This work was supported by NASA Grant NAGW-1855.

REFERENCES

Case, R.A., and H.P. Gerrish, 1988: Annual Summary Atlantic Hurricane Season of 1987. Mon. Wea. Rev., 116, 939-949.

Ferrier, B.S., and R.A. Houze, Jr., 1989: One-dimensional time-dependent modeling of deep convection. Part I: Model dynamics and simulations of GATE cumulonimbus clouds. J. Atmos. Sci., 46, 330-352.

Grody, N.C., 1988: Surface identification using satellite microwave radiometers. IEEE Trans. on Geoscience and Rem. Sensing, 26, 850-859.

Hollinger, J.P. (ed.), 1991: DMSP Special Sensor Microwave/Imager Calibration/Validation Final Report Volume I. Naval Research Laboratory, Washington, D.C.

Keenan, T.D., G.J. Holland, M.J. Manton, and J. Simpson, 1988: TRMM ground truth in a monsoon environment: Darwin, Australia. Aust. Met. Mag., 36, 81-90.

Kummerow, C., R.A. Mack, and I.M.Hakkarinen, 1989: A self-consistency approach to improve microwave rainfall rate estimation from space. J. Appl. Meteor., 28, 869-884.

López, R.E., 1977: The lognormal distribution and cumulus cloud populations. Mon. Wea. Rev., 105, 865-872.

Lorenc, A.C., 1986: Analysis methods for numerical weather prediction. Quart. J. R. Met. Soc., 112, 1177-1194.

Petty, G.W., and K.B. Katsaros, 1990: New geophysical algorithms for the Special Sensor Microwave Imager. Fifth International Conference on Satellite Meteorology and Oceanography, September 3-7, London, England, 247-251.

Pickard, G.L. and W.J. Emery, 1982: Descriptive Physical Oceanography. Pergamon Press, New York, 249 pp.

Ridout, J.A., 1991: A Parameterized Quasi-Five-Cylinder Convective Cloud Model and Its Application to Remote Sensing of Rainfall. Ph.D. thesis, University of Wisconsin, Madison, Wisconsin, 278 pp.

Ridout, J. A., 1993: A quasi-five-cylinder model of deep convection. Part I: Updraft growth in non-sheared environments. Submitted to J. Atmos. Sci..

Shanno, D.F., 1978: Conjugate gradient methods with inexact searches. Math. Oper. Res., 3, 244-256.

Schoeberl, M., J. Pfaendtner, R. Rood, A. Thompson, and B. Wielicki, 1992: Atmospheres panel report to the payload panel. Paleogeography, Paleoclimatology, Paleoecology (Global and Planetary Change Section), 98, 9-23.

Short, D.A., 1988: A statistical-physical interpretation of ESMR-5 brightness temperatures over the GATE area. In Tropical Rainfall Measurements, Proceedings of the International Symposium on Tropical Precipitation Measurements, Tokyo. A. Deepak Publishing, Hampton, Virginia.

Simpson, J., R.F. Adler, G.R. North, 1988: A proposed Tropical Rainfall Measuring Mission (TRMM) Satellite. Bull. Amer. Met. Soc., 69, 278-295.

Smith, W.L., H.M. Woolf, P.G. Abel, C.M. Hayden, M. Chalfant, and N. Grody, 1974: Nimbus-5 sounder data processing system Part I: Measurement characteristics and data reduction procedures. NOAA Technical Memorandum NESS 57, 99 pp.

Xiang, X., E.A. Smith, and G.J. Tripoli, 1992: A cloud and radiation model-based algorithm for rainfall retrieval from SSM/I multispectral microwave measurements. Proceedings of the Sixth Conference on Satellite Meteorology and Oceanography, Atlanta, Georgia, 286-289.

Table 1. Retrieved geophysical parameters (**P**) and associated spatial constraints in the SSM/I physical retrieval method.

Parameter	Spatial Constraints
land fraction within each grid box	none
land emissivity parameters from Grody (1988) parameterization	uniform over grid
ocean emissivity parameters from Grody (1988) parameterization	uniform over grid
first eigenfunction weight of water vapor mixing ratio profile	uniform over land, no constraint over ocean
precipitation fraction within each grid box	none
mean slant path depth of precipitating liquid within the precipitation fraction	none
mean slant path depth of precipitating ice within the precipitation fraction	none

(a)

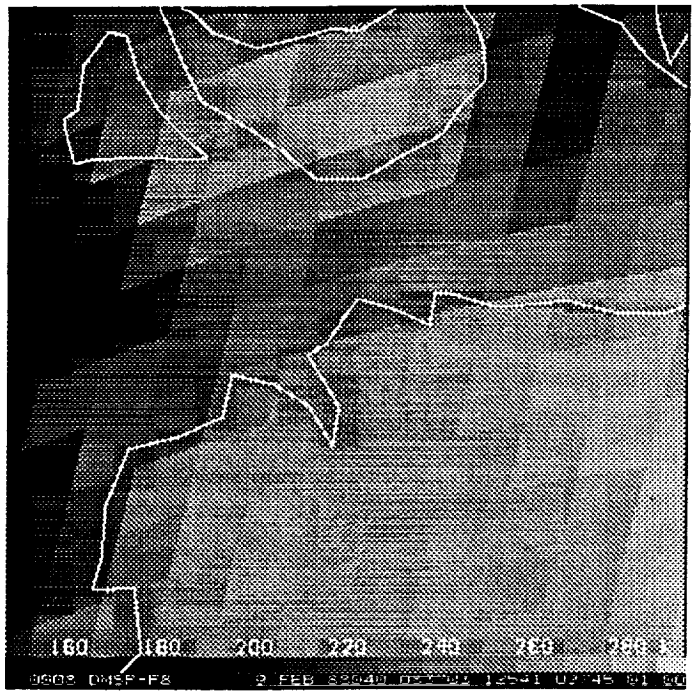

(b)

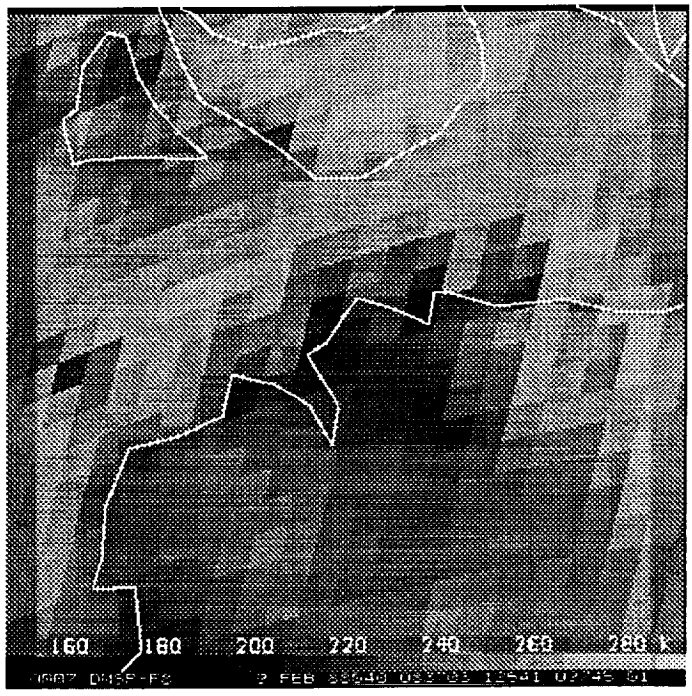

Fig. 1. SSM/I antenna temperature imagery of a tropical squall line in the vicinity of Darwin, Australia at 0906 UTC on February 9, 1988. The 37 GHz horizontal polarization imagery is shown in panel (a), and the 85.5 GHz horizontal polarization imagery is shown in panel (b). Coastlines are indicated by solid white lines. The area represented by each panel is approximately 250 km x 250 km.

(a)

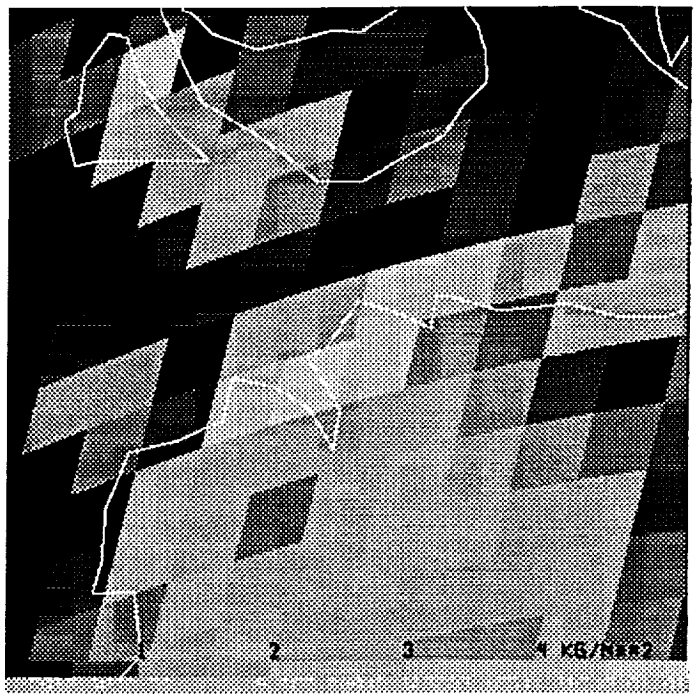

(b)

Fig. 2. Retrieved distributions of slant path-integrated precipitating liquid (a) and ice (b) derived from the SSM/I overpass of Darwin, Australia at 0906 UTC on February 9, 1988.

(a)

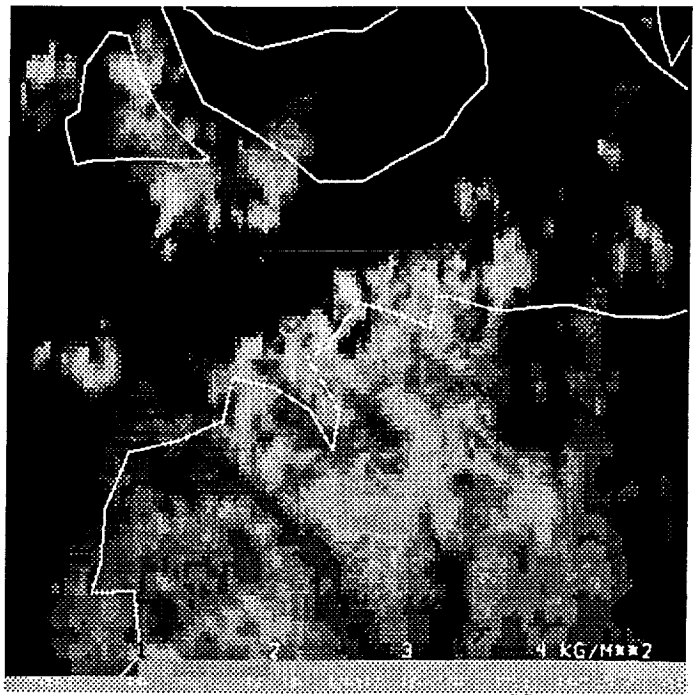

(b)

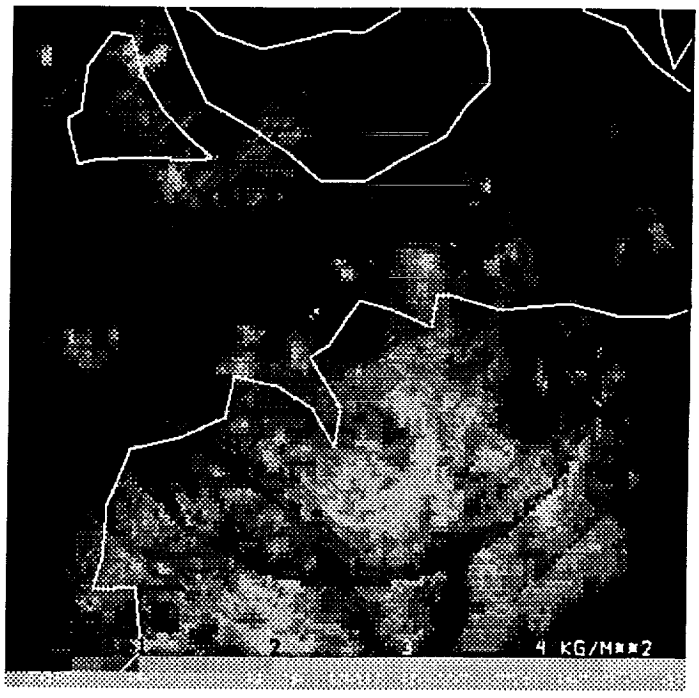

Fig. 3. Distributions of slant path-integrated precipitating liquid (a) and ice (b) derived from a volume scan of the Darwin/TOGA radar starting at 0850 UTC on February 9, 1988.

(a)

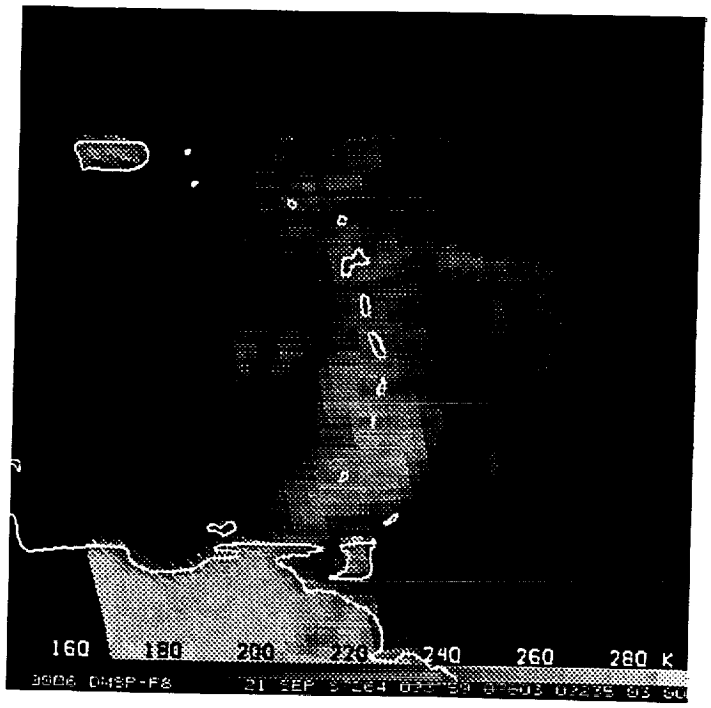

(b)

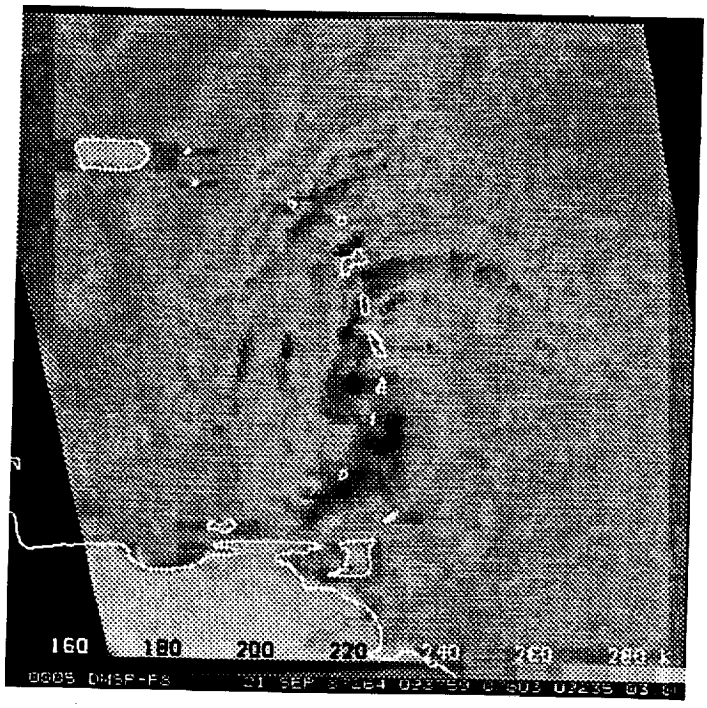

Fig. 4. SSM/I antenna temperature imagery of Tropical Storm Emily in the Windward Islands at 1004 UTC on September 21, 1987. The 37 GHz horizontal polarization imagery is shown in panel (a), and the 85.5 GHz horizontal polarization imagery is shown in panel (b). Coastlines are indicated by solid white lines. The area represented by each panel is approximately 1500 km x 1500 km.

(a)

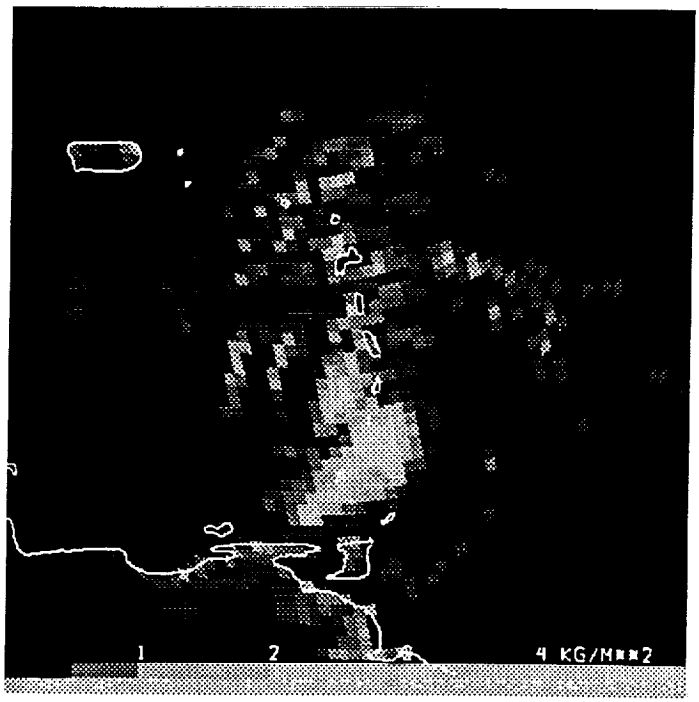

(b)

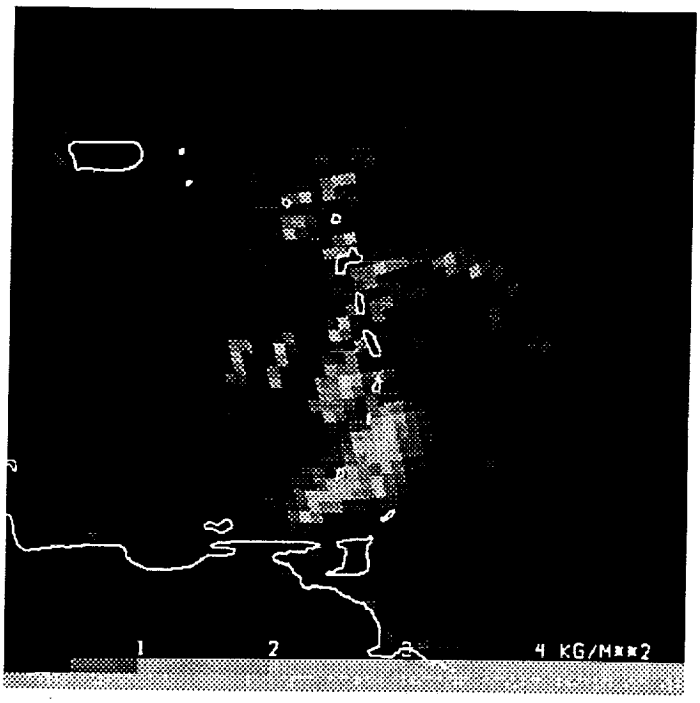

Fig. 5. Retrieved distributions of slant path-integrated precipitating liquid (a) and ice (b) derived from the SSM/I overpass of Tropical Storm Emily at 1004 UTC on September 21, 1987.

(a)

(b)

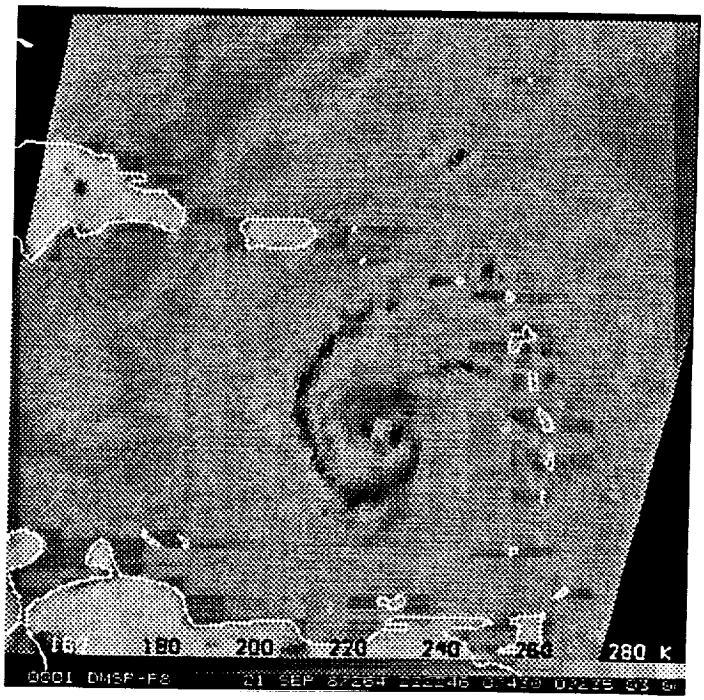

Fig. 6. SSM/I antenna temperature imagery of Tropical Storm Emily north of Venezuela at 2242 UTC on September 21, 1987. The 37 GHz horizontal polarization imagery is shown in panel (a), and the 85.5 GHz horizontal polarization imagery is shown in panel (b). Coastlines are indicated by solid white lines. The area represented by each panel is approximately 1500 km x 1500 km.

(a)

(b)

Fig. 7. Retrieved distributions of slant path-integrated precipitating liquid (a) and ice (b) derived from the SSM/I overpass of Tropical Storm Emily at 2242 UTC on September 21, 1987.